CRNOGORSKA AKADEMIJA NAUKA I UMJETNOSTI
GLASNIK ODJELJENJA PRIRODNIH NAUKA, 20, 2014.

QERNOGORSKAYA AKADEMIYA NAUK I ISSKUSTV
GLASNIK OTDELENIYA ESTESTVENNYH NAUK, 20, 2014.

THE MONTENEGRIN ACADEMY OF SCIENCES AND ARTS
PROCEEDINGS OF THE SECTION OF NATURAL SCIENCES, 20, 2014

UDK 539.319

*Vlado A. Lubarda**

ELASTIC RESPONSE OF CURVILINEARLY ANISOTROPIC NONUNIFORM SOLID OR HOLLOW DISK, CYLINDER AND SPHERE

A b s t r a c t

Recent analysis [1] of the pressurized radially nonuniform, curvilinearly anisotropic hollow disk, cylinder, and sphere is extended to encompass the displacement and two types of mixed boundary conditions. The pressurized solid disk, cylinder, and sphere are then considered, with a small pith around their centers, made of a material with elastic properties different from the surrounding material, to eliminate the stress and displacement singularities at the center. The results are applied to a thin cylindrically orthotropic disk made of hardwood red oak. The discontinuity in hoop stress across the pith-interface is discussed.

ELASTIČNOST NEHOMOGENOG, KRIVOLINIJSKI ANIZOTROPNOG DISKA, CILINDRA I KUGLE

I z v o d

U radu je proširena ranija autorova analiza [1] nehomogenog, krivolinijski anizotropnog šupljeg diska, cilindra i kugle pod uticajem ravnomjernog

*Prof. dr V.A. Lubarda, The Montenegrin Academy of Sciences and Arts, 81000 Podgorica, Montenegro, and University of California, San Diego, CA 92093-0411, USA.

pritiska po unutrašnjoj i spoljnoj površini, uključivanjem u analizu graničnih uslova po pomjeranjima i mješovitih graničnih uslova. Dobijeni rezultati su primijenjeni na naponsku i deformacionu analizu punog diska, cilindra i kugle, sa centralnim jezgrom (inkluzijom) od materijala različitih elastičnih svojstava od okolnog materijala, neophodnog da bi se izbjegla singularnost napona i pomjeranja. Diskutovan je diskontinuitet transverzalne komponente normalnog napona, zavisno od diskontinuiteta modula elastičnosti, sa primjenom na model hrastovog drveta.

1. INTRODUCTION

In a recent paper we presented a unified analysis of elastic response of a pressurized cylindrically anisotropic (locally orthotropic) hollow disk (plane stress) or hollow cylinder (plane strain), and a spherically anisotropic (locally transversely isotropic) hollow sphere, made of a material which is nonuniform in the radial direction according to a power law relationship. Such analysis is of importance for the evaluation of stress amplification or shielding caused by curvilinear anisotropy or radial nonuniformity of the material. The results can be used for material tailoring and optimization of machine components and structural elements made from functionally graded materials. The effects of curvilinear anisotropy and radial nonuniformity on the stress response in structural mechanics have been studied extensively in the past. The early work includes the contributions [2-6]. The topic regained attention in the sequence of publications [7-24]. In the present paper we extend the analysis from [1], which was restricted to stress boundary conditions, to encompass the hollow disks, cylinders and spheres under displacement and two types of mixed boundary conditions. Further extension of the analysis to a generalized plane stress and generalized plane strain is also possible. The solid disk, cylinder, and sphere are then considered, with a small pith around their centers having different elastic properties from the surrounding material, to eliminate the stress and displacement singularities at the center. The results are applied to a pressurized thin disk made of hardwood red oak. The discontinuity in hoop stress across the pith-interface is discussed.

2. CURVILINEAR ANISOTROPY AND RADIAL NONUNIFORMITY

Consider a cylindrically anisotropic disk (plane stress) or cylinder (plane strain), made of the material which is locally orthotropic, with the principal axes of orthotropy in the (r, θ, z) directions, and a spherically anisotropic sphere which is at any point transversely isotropic around the radial direction. The corresponding stress-strain relations for infinitesimally small elastic deformations are

$$\epsilon_r = \frac{1}{E_\theta}(\alpha\sigma_r - j\beta\sigma_\theta)\,, \quad \epsilon_\theta = \frac{1}{E_\theta}(\gamma\sigma_\theta - \beta\sigma_r)\,, \tag{2.1}$$

where $j = 1$ for a disk and cylinder, and $j = 2$ for a sphere. The material parameters (α, β, γ) were introduced in [1] as

$$\alpha = \begin{cases} k, \\ k(1 - \nu_{rz}\nu_{zr}), \\ k, \end{cases} \quad \beta = \begin{cases} \nu_{\theta r}, & \text{for a disk,} \\ \nu_{\theta r} + \nu_{\theta z}\nu_{zr}, & \text{for a cylinder,} \\ \nu_{\theta r}, & \text{for a sphere,} \end{cases} \tag{2.2}$$

and

$$\gamma = \begin{cases} 1, & \text{for a disk,} \\ 1 - \nu_{z\theta}\nu_{\theta z}, & \text{for a cylinder,} \\ 1 - \nu_{\phi\theta}, & \text{for a sphere.} \end{cases} \tag{2.3}$$

The coefficient $k = E_\theta/E_r$ specifies the degree of in-plane anisotropy of elastic moduli. The coefficient of lateral contraction $\nu_{\theta r}$ stands for the coefficient of lateral contraction in the r-direction due to stress in the θ-direction, and likewise for other coefficients of lateral contraction. In the case of cylindrical anisotropy, the coefficients of lateral contraction are related by the symmetry relations $E_r\nu_{\theta r} = E_\theta\nu_{r\theta}$, $E_\theta\nu_{z\theta} = E_z\nu_{\theta z}$, and $E_z\nu_{rz} = E_r\nu_{zr}$.

By the positive-definiteness of the strain energy function, the elastic moduli are positive and the coefficients of lateral contraction are constrained by

$$\begin{aligned} &0 < \nu_{r\theta}\nu_{\theta r} < 1\,, \quad 0 < \nu_{\theta z}\nu_{z\theta} < 1\,, \quad 0 < \nu_{zr}\nu_{rz} < 1\,, \\ &\nu_{r\theta}\nu_{\theta r} + \nu_{\theta z}\nu_{z\theta} + \nu_{zr}\nu_{rz} + \nu_{rz}\nu_{z\theta}\nu_{\theta r} + \nu_{zr}\nu_{\theta z}\nu_{r\theta} < 1\,. \end{aligned} \tag{2.4}$$

The constraint $0 < \nu_{r\theta}\nu_{\theta r} < 1$ sets the bounds on $\nu_{\theta r}$ and $\nu_{r\theta}$ to be $|\nu_{\theta r}| < k^{1/2}$ and $|\nu_{r\theta}| < k^{-1/2}$, both coefficients being simultaneously either positive or negative. For spherical anisotropy, the conditions (2.4) reduce to

$$-1 < \nu_{\phi\theta} < 1\,, \quad \nu_{r\theta}\nu_{\theta r} < 1\,, \quad \nu_{\phi\theta} + 2\nu_{r\theta}\nu_{\theta r} < 1\,. \tag{2.5}$$

In addition to the described anisotropy properties, it will be assumed that a considered disk, cylinder or sphere are made of a material which is nonuniform in the radial direction, such that its elastic moduli vary in the radial direction according to the power-law relations

$$E_r = E_r^b \left(\frac{r}{b}\right)^m, \quad E_\theta = E_\theta^b \left(\frac{r}{b}\right)^m, \quad E_z = E_z^b \left(\frac{r}{b}\right)^m. \tag{2.6}$$

The exponent m is a real number, reflecting the degree of nonuniformity of the material, and $(E_r^b, E_\theta^b, E_z^b)$ are the elastic moduli at the outer boundary $r = b$. The same m is used for all three muduli, so that the ratios of the moduli in different directions are constant, e.g., $E_\theta/E_r = E_\theta^b/E_r^b = k =$ const. All coefficients of lateral contraction are assumed to be independent of r, which considerably simplifies the mathematical aspects of the analysis and is in accord with the assumption commonly used in the mechanics of functionally graded materials [12,18,23].

3. GOVERNING DIFFERENTIAL EQUATION

In the absence of body force, the equilibrium equation is

$$\frac{\mathrm{d}\sigma_r}{\mathrm{d}r} + j\,\frac{\sigma_r - \sigma_\theta}{r} = 0\,. \tag{3.1}$$

Denoting by $u = u(r)$ the radial displacement, the strain-displacement relations are $\epsilon_r = \mathrm{d}u/\mathrm{d}r$ and $\epsilon_\theta = u/r$. The corresponding Saint-Venant compatibility condition is

$$\frac{\mathrm{d}\epsilon_\theta}{\mathrm{d}r} + \frac{\epsilon_\theta - \epsilon_r}{r} = 0\,. \tag{3.2}$$

By substituting the stress-strain relations (2.1) into (3.2), and by using the equilibrium equation (3.1), the Beltrami–Michell compatibility condition is found to be

$$\frac{\mathrm{d}\sigma_\theta}{\mathrm{d}r} + \frac{1}{r}\left[(1-m)\sigma_\theta - \varphi\sigma_r\right] = 0\,, \tag{3.3}$$

where

$$\varphi = \frac{1}{\gamma}\left[\alpha + \beta(1-j)\right] - m\,\frac{\beta}{\gamma}\,. \tag{3.4}$$

The parameter φ accounts for the combined effects of the state of anisotropy, represented by the parameters (α, β, γ) and the degree of nonuniformity, represented by the parameter m [1].

Upon differentiating (3.1) and by using (3.3), there follows

$$r^2\,\frac{\mathrm{d}^2\sigma_r}{\mathrm{d}r^2} + (2+j-m)r\,\frac{\mathrm{d}\sigma_r}{\mathrm{d}r} + j(1-m-\varphi)\sigma_r = 0\,. \tag{3.5}$$

The solution of (3.5) is

$$\sigma_r = Ar^{-n_1} + Br^{-n_2}\,, \tag{3.6}$$

where A and B are the integration constants, and

$$n_{1,2} = \frac{1}{2}\,(1+j-m\mp s)\,, \quad s = \left[(1+j-m)^2 - 4j(1-\varphi-m)\right]^{1/2}\,. \tag{3.7}$$

Having established the expression (3.6) for the radial stress, the circumferential stress follows from (3.1) as

$$\sigma_\theta = \left(1-\frac{n_1}{j}\right)Ar^{-n_1} + \left(1-\frac{n_2}{j}\right)Br^{-n_2}\,. \tag{3.8}$$

The substitution of (3.6) and (3.8) into the second of (2.1) yields an expression for the circumferential strain ϵ_θ, and thus the displacement expression as $u = r\epsilon_\theta$. The result is

$$u = \frac{b}{E_\theta^b}\left(\frac{b}{r}\right)^{m-1}\left(\eta_1 Ar^{-n_1} + \eta_2 Br^{-n_2}\right). \tag{3.9}$$

where

$$\eta_1 = \gamma\left(1-\frac{n_1}{j}\right) - \beta\,, \quad \eta_2 = \gamma\left(1-\frac{n_2}{j}\right) - \beta\,. \tag{3.10}$$

For uniform isotropic material, the parameters η_1 and η_2 become

$$\eta_1 = \gamma\left(1+\frac{1}{j}\right) + \eta_2\,, \quad \eta_2 = -\frac{1}{j}\,(1+\nu)\,, \tag{3.11}$$

where $\gamma = 1$ for a disk, $\gamma = 1-\nu^2$ for a cylinder, and $\gamma = 1-\nu$ for a sphere.

In the case of a thin disk under plane stress conditions, the resulting strain ϵ_z is in general not constant (as in the case of uniform isotropic disk), but r-dependent, which means that the obtained plane stress solution is only approximate. The generalized plane stress and plane strain conditions were examined in detail in [1].

4. PRESCRIBED PRESSURE AT BOTH BOUNDARIES

When the uniform pressures p and q are applied at the inner and outer boundary, $\sigma_r(a) = -p$ and $\sigma_r(b) = -q$, the integration constants in (3.6) become

$$A = \frac{pc^{n_2} - q}{1-c^s}\, b^{n_1}\,, \quad B = \frac{pc^{n_1} - q}{1-c^{-s}}\, b^{n_2}\,, \tag{4.1}$$

where $c = a/b$. Consequently, the radial and hoop stresses are

$$\sigma_r(r) = \frac{pc^{n_2} - q}{1-c^s}\left(\frac{b}{r}\right)^{n_1} + \frac{pc^{n_1} - q}{1-c^{-s}}\left(\frac{b}{r}\right)^{n_2}\,, \tag{4.2}$$

$$\sigma_\theta(r) = \left(1-\frac{n_1}{j}\right)\frac{pc^{n_2} - q}{1-c^s}\left(\frac{b}{r}\right)^{n_1} + \left(1-\frac{n_2}{j}\right)\frac{pc^{n_1} - q}{1-c^{-s}}\left(\frac{b}{r}\right)^{n_2}\,. \tag{4.3}$$

The corresponding radial displacement is

$$u(r) = \frac{b}{E_\theta^b}\left[\eta_1\,\frac{pc^{n_2} - q}{1-c^s}\left(\frac{b}{r}\right)^{m+n_1-1} + \eta_2\,\frac{pc^{n_1} - q}{1-c^{-s}}\left(\frac{b}{r}\right)^{m+n_2-1}\right]. \tag{4.4}$$

4.1. Internal Pressure Only

By substituting $q = 0$ in the general expressions (4.2)–(4.4), the stresses are found to be

$$\sigma_r(r) = \left[\frac{c^s}{1-c^s}\left(\frac{a}{r}\right)^{n_1} + \frac{c^{-s}}{1-c^{-s}}\left(\frac{a}{r}\right)^{n_2}\right]p\,, \tag{4.5}$$

$$\sigma_\theta(r) = \left[\left(1-\frac{n_1}{j}\right)\frac{c^s}{1-c^s}\left(\frac{a}{r}\right)^{n_1} + \left(1-\frac{n_2}{j}\right)\frac{c^{-s}}{1-c^{-s}}\left(\frac{a}{r}\right)^{n_2}\right]p\,. \tag{4.6}$$

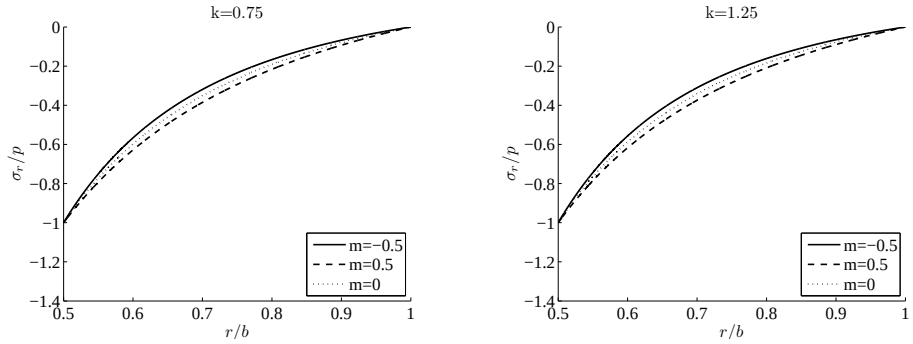

(a) (b)

Figure 1: The variation of the radial stress for (a) $k = 0.75$ and (b) $k = 1.25$, in the case of internal pressure alone ($q = 0$). The aspect ratio of the disk is $c = a/b = 0.5$ and the parameters $\beta = 0.35$ and $\gamma = 1$.

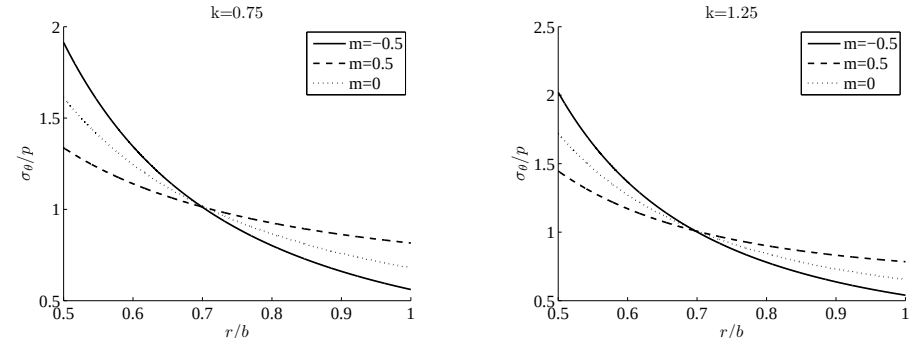

(a) (b)

Figure 2: The variation of the circumferential stress for (a) $k = 0.75$ and (b) $k = 1.25$, in the case of internal pressure alone ($q = 0$). The aspect ratio of the disk is $c = a/b = 0.5$ and the parameters $\beta = 0.35$ and $\gamma = 1$.

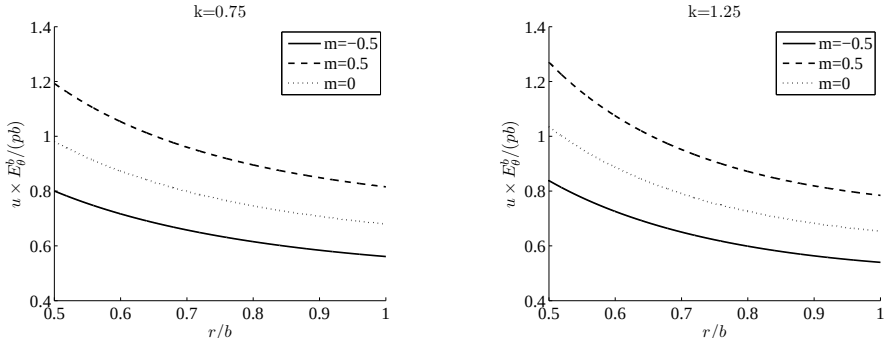

(a) (b)

Figure 3: The variation of the radial displacement for (a) $k = 0.75$ and (b) $k = 1.25$, in the case of internal pressure alone ($q = 0$). The aspect ratio of the disk is $c = a/b = 0.5$ and the parameters $\beta = 0.35$ and $\gamma = 1$.

The radial displacement is

$$u(r) = \left[\eta_1 \frac{c^s}{1-c^s}\left(\frac{a}{r}\right)^{m+n_1-1} + \eta_2 \frac{c^{-s}}{1-c^{-s}}\left(\frac{a}{r}\right)^{m+n_2-1}\right] \frac{pa}{E_\theta^a}\,. \tag{4.7}$$

While the radial dependence of stress is governed by the exponents n_1 and n_2, the radial dependence of the displacement response is governed by the exponents $m + n_1 - 1$ and $m + n_2 - 1$. Figures 1–3 show the plots of the normalized stress components and the displacement versus the normalized radius in a hollow disk with the aspect ratio $c = a/b = 0.5$. The state of elastic anisotropy is such that $\beta = 0.35$ and $\gamma = 1$. Parts (a) of the figures are for $\alpha = k = 0.75$ and parts (b) for $\alpha = k = 1.25$. The three curves in each plot correspond to three selected values of the nonuniformity parameter m. As seen from the figures, the hoop stress $\sigma_\theta(a)$ decreases with the increasing value of m, and is in each case greater for $k = 1.25$ than for $k = 0.75$. On the other hand, the radial displacement increases with the increasing value of m, and $u(a)$ in each case is greater for $k = 1.25$ than for $k = 0.75$. A more general parametric study could be performed by varying the value of s around $s = 2$, for each value of m around $m = 0$. Such study may be of interest for the material and structural optimization analysis [8].

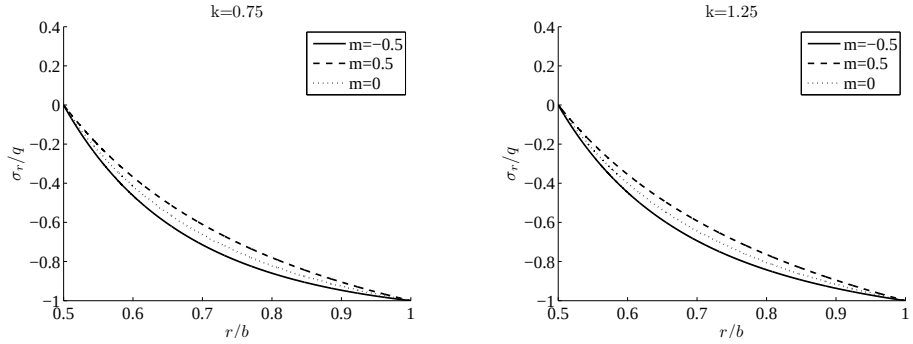

(a) (b)

Figure 4: The variation of the radial stress for (a) $k = 0.75$ and (b) $k = 1.25$, in the case of external pressure alone ($p = 0$).

4.2. External Pressure Only

If $p = 0$ is substituted in (4.2)–(4.4), the stresses become

$$\sigma_r(r) = \left[\frac{1}{c^s - 1}\left(\frac{b}{r}\right)^{n_1} + \frac{1}{c^{-s} - 1}\left(\frac{b}{r}\right)^{n_2}\right] q\,, \tag{4.8}$$

$$\sigma_\theta(r) = \left[\left(1 - \frac{n_1}{j}\right)\frac{1}{c^s - 1}\left(\frac{b}{r}\right)^{n_1} + \left(1 - \frac{n_2}{j}\right)\frac{1}{c^{-s} - 1}\left(\frac{b}{r}\right)^{n_2}\right] q\,, \tag{4.9}$$

while the radial displacement is

$$u(r) = \left[\eta_1 \frac{1}{c^s - 1}\left(\frac{b}{r}\right)^{m+n_1-1} + \eta_2 \frac{1}{c^{-s} - 1}\left(\frac{b}{r}\right)^{m+n_2-1}\right] \frac{qb}{E_\theta^b}\,. \tag{4.10}$$

Figures 4–6 show the stress and displacement variations for the same material parameters as used to construct Figures 1–3. The magnitude of the hoop stress $\sigma_\theta(a)$ decreases with the increasing value of m, and in each case is smaller for $k = 1.25$ than for $k = 0.75$.

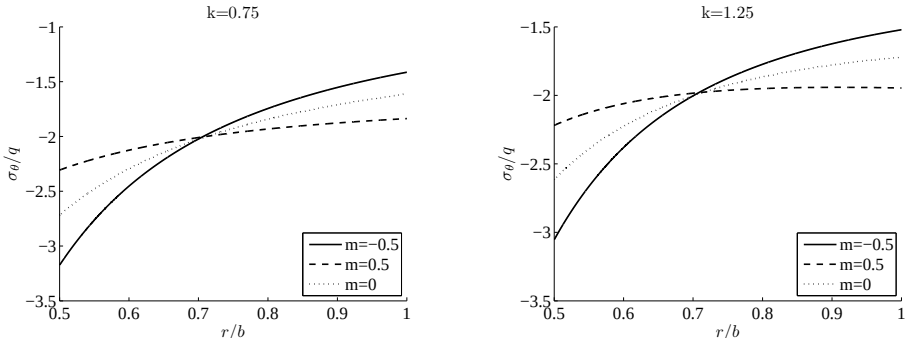

(a) (b)

Figure 5: The variation of the circumferential stress for (a) $k = 0.75$ and (b) $k = 1.25$, in the case of external pressure alone ($p = 0$).

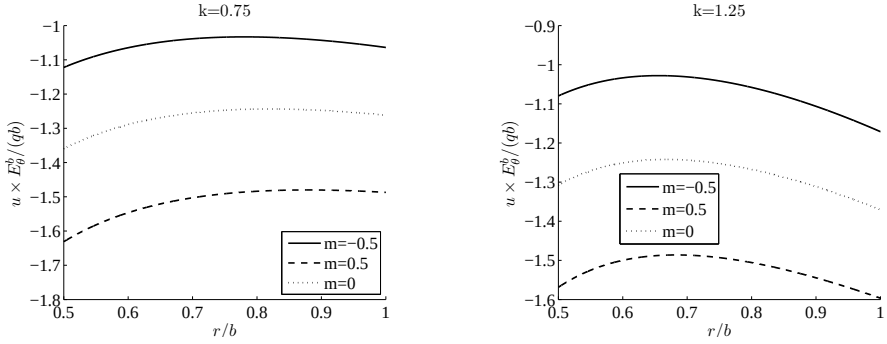

(a) (b)

Figure 6: The variation of the radial displacement for (a) $k = 0.75$ and (b) $k = 1.25$, in the case of external pressure alone ($p = 0$).

The normalized circumferential stress and the (inward) displacement at $r = a$ are

$$\frac{\sigma_\theta(a)}{q} = \frac{s}{j}\,\frac{c^{-n_1}}{c^s - 1}\,, \quad -\frac{u(a)}{a} = \frac{\gamma s/j}{1 - c^s}\,c^{-(n_1+m)}\,\frac{q}{E^b_\theta}\,. \tag{4.11}$$

For a very small hole ($c \ll 1$), they become

$$\frac{\sigma_\theta(a)}{q} \approx -\frac{s}{j}\,c^{-n_1}\,, \quad -\frac{u(a)}{a} = \frac{\gamma s}{j}\,c^{-(n_1+m)}\,\frac{q}{E^b_\theta}\,. \tag{4.12}$$

Consequently, if $n_1 < 0$ the stress concentration factor diminishes to zero (stress shielding); if $n_1 > 0$, the stress concentration factor increases to infinity (stress amplification). If $n_1 = 0$, the stress concentration factor approaches the value s/j. The material interpenetration, in the sense of [25], does not occur if $n_1 + m < 0$.

5. PRESCRIBED DISPLACEMENT AT BOTH BOUNDARIES

If the displacements are prescribed at both boundaries, such that $u(a) = u_a$ and $u(b) = u_b$, the integration constants in (3.9) are found to be

$$\begin{aligned} A &= \frac{1}{\eta_1}\,\frac{1}{a^s - b^s}\left[a^{n_2}E^a_\theta(u_a/a) - b^{n_2}E^b_\theta(u_b/b)\right], \\ B &= -\frac{1}{\eta_2}\,\frac{a^s b^s}{a^s - b^s}\left[a^{n_1}E^a_\theta(u_a/a) - b^{n_1}E^b_\theta(u_b/b)\right], \end{aligned} \tag{5.1}$$

where $E^a_\theta = (a/b)^m E^b_\theta$. Figures 7–9 show the results for $u_a = u_b = 10^{-3}b$ and for the same material properties as used to construct other figures in this paper. For example, in case ($m = -0.5$, $k = 0.75$), the radial stress $\sigma_r(a)$ is tensile, while in case ($m = -0.5$, $k = 1.25$) it is compressive. In all cases shown in Fig. 7 the radial stress $\sigma_r(b)$ is tensile, as expected for the prescribed positive (outward) displacements $u_a = u_b = 10^{-3}b$. Figure 9 shows that the minimum radial displacement in the disk is smaller for $k = 1.25$ than for $k = 0.75$. Clearly, one can optimize the material properties in order to achieve a desired stiffness or compliance in the response of the disk.

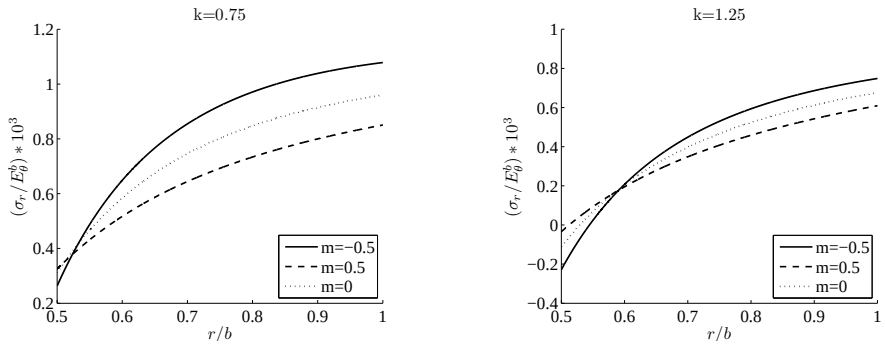

(a) (b)

Figure 7: The variation of the radial stress for (a) $k = 0.75$ and (b) $k = 1.25$ under prescribed displacements $u_a = u_b = 10^{-3}b$.

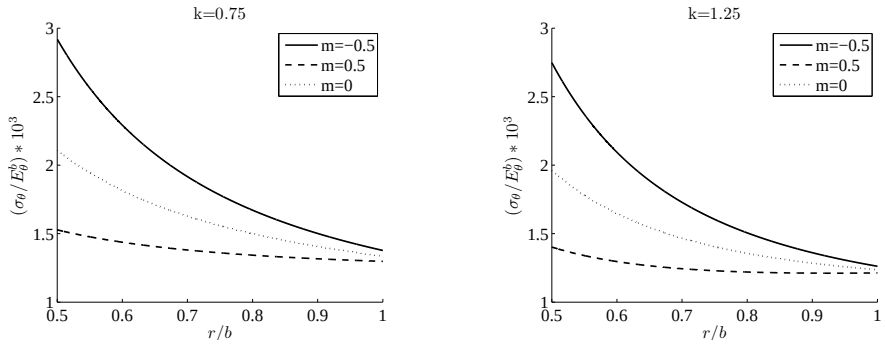

(a) (b)

Figure 8: The variation of the circumferential stress for (a) $k = 0.75$ and (b) $k = 1.25$ under prescribed displacements $u_a = u_b = 10^{-3}b$.

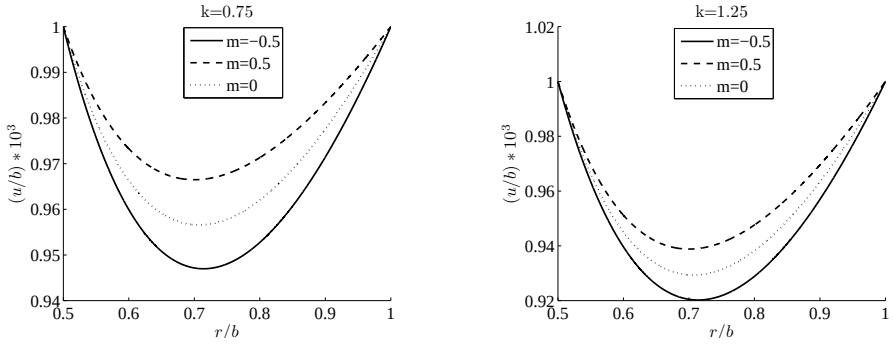

(a) (b)

Figure 9: The variation of the radial displacement for (a) $k = 0.75$ and (b) $k = 1.25$ under prescribed displacements $u_a = u_b = 10^{-3}b$.

6. MIXED BOUNDARY CONDITIONS

6.1. Prescribed Displacement at the Inner and Pressure at the Outer Boundary

For the mixed-type boundary conditions when displacement is applied at the inner and pressure at the outer boundary, $u(a) = u_a$ and $\sigma_r(b) = -q$, the integration constants are

$$\begin{aligned} A =& \frac{1}{\eta_1 a^s - \eta_2 b^s} \left[a^{n_2} E_\theta^a (u_a/a) + \eta_2 b^{n_2} q\right], \\ B =& -\frac{a^s b^s}{\eta_1 a^s - \eta_2 b^s} \left[a^{n_1} E_\theta^a (u_a/a) + \eta_1 b^{n_1} q\right]. \end{aligned} \tag{6.1}$$

Figures 10–12 show the results for $u_a = 0$ and $q = 10^{-3} E_\theta^b$. Higher pressure at the inner boundary $\sigma_r(a)$ is required to keep $u(a) = 0$ in case $k = 0.75$ than $k = 1.25$ (Fig. 10), while larger inward displacement $u(b)$ is produced in case $k = 1.25$ than $k = 0.75$ (Fig. 12). The magnitude of the hoop stress $\sigma_\theta(a)$ is greater, while the magnitude of the hoop stress $\sigma_\theta(b)$ is smaller for $k = 0.75$ than for $k = 1.25$ (Fig. 11). In each case, the magnitude of the hoop stress $\sigma_\theta(a)$ is greater for $m = 0.5$ than for $m = -0.5$, while the magnitude of $\sigma_\theta(b)$ is smaller for $m = 0.5$ that for $m = -0.5$.

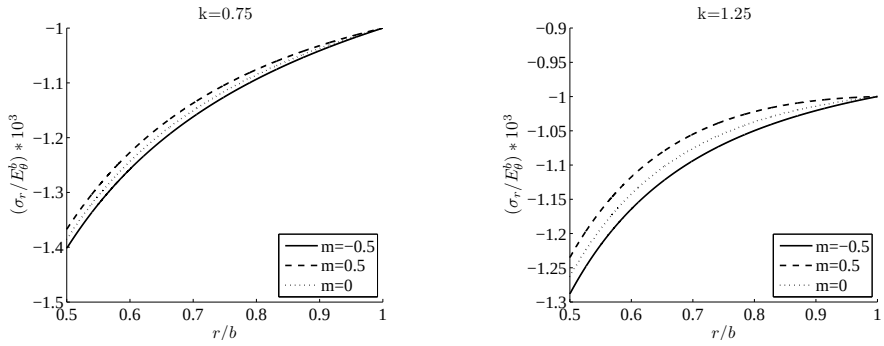

(a) (b)

Figure 10: The variation of the radial stress for (a) $k = 0.75$ and (b) $k = 1.25$ under prescribed displacement $u_a = 0$ and pressure $q = 10^{-3}E_\theta^b$.

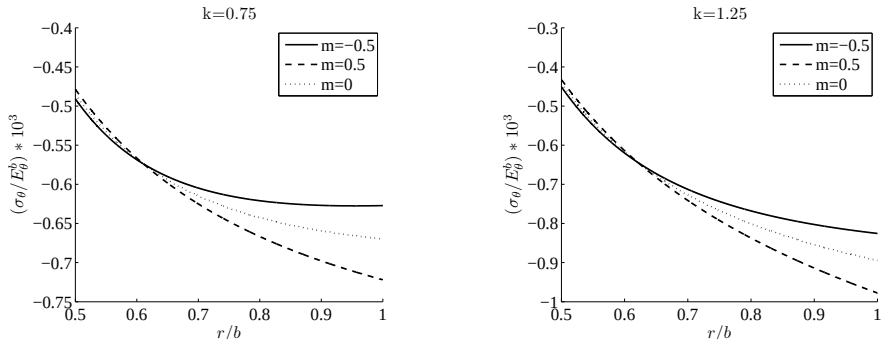

(a) (b)

Figure 11: The variation of the circumferential stress for (a) $k = 0.75$ and (b) $k = 1.25$ under prescribed displacement $u_a = 0$ and pressure $q = 10^{-3}E_\theta^b$.

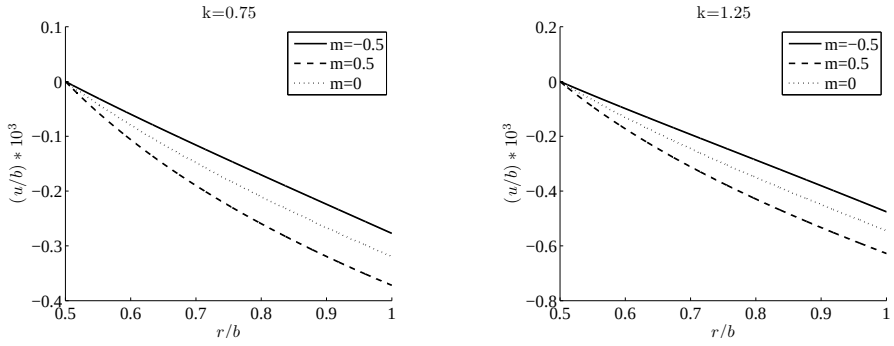

(a) (b)

Figure 12: The variation of the radial displacement for (a) $k = 0.75$ and (b) $k = 1.25$ under prescribed displacement $u_a = 0$ and pressure $q = 10^{-3}E_\theta^b$.

6.2. Prescribed Pressure at the Inner and Displacement at the Outer Boundary

The second type of the mixed boundary conditions corresponds to prescribed pressure at the inner and displacement at the outer boundary, such that $\sigma_r(a) = -p$ and $u(b) = u_b$. In this case, the integration constants are found to be

$$\begin{aligned} A &= \frac{1}{\eta_1 b^s - \eta_2 a^s}\left[\eta_2 a^{n_2} p + b^{n_2} E_\theta^b (u_b/b)\right], \\ B &= -\frac{a^s b^s}{\eta_1 b^s - \eta_2 a^s}\left[\eta_1 a^{n_1} p + b^{n_1} E_\theta^b (u_b/b)\right]. \end{aligned} \tag{6.2}$$

Figures 13–15 show the results for $u_b = 0$ and $p = 10^{-3}E_\theta^b$. Higher pressure at the outer boundary $\sigma_r(b)$ is required to keep $u(b) = 0$ in case $k = 0.75$ than $k = 1.25$ (Fig. 13), while larger outward displacement $u(a)$ is produced in case $k = 1.25$ than $k = 0.75$ (Fig. 15). The hoop stress $\sigma_\theta(a)$ is greater for $k = 1.25$ than $k = 0.75$ (Fig. 14).

7. SOLID DISK, CYLINDER, AND SPHERE

If there is no central whole ($a = 0$), the power-law relations (2.6) hold for $r > a_o$, where a_o is the radius of a small circle (pith) around the axis of

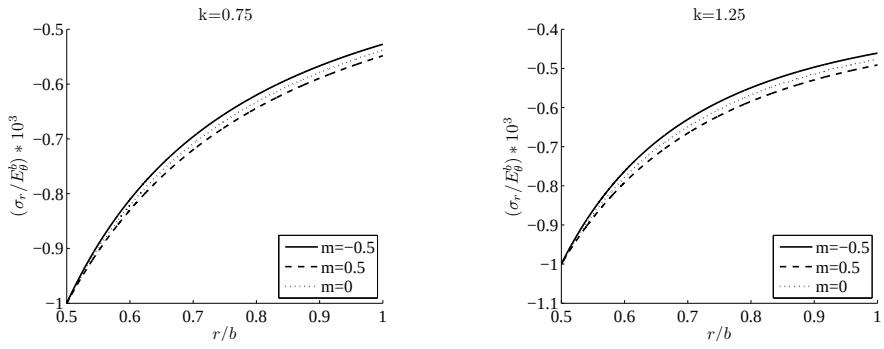

(a) (b)

Figure 13: The variation of the radial stress for (a) $k = 0.75$ and (b) $k = 1.25$ under prescribed pressure $p = 10^{-3}E_\theta$ and displacement $u_b = 0$.

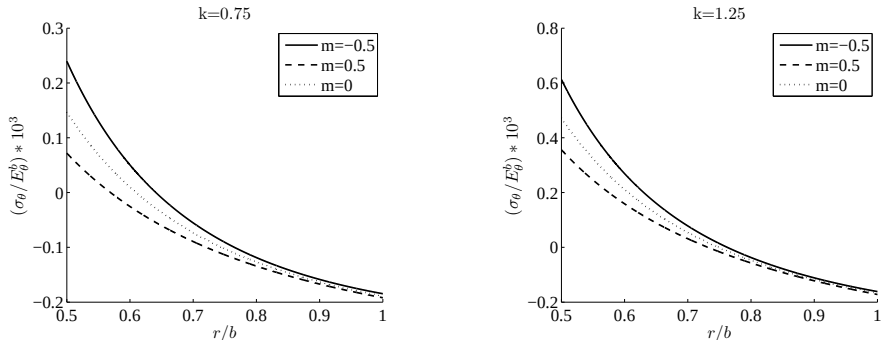

(a) (b)

Figure 14: The variation of the circumferential stress for (a) $k = 0.75$ and (b) $k = 1.25$ under prescribed pressure $p = 10^{-3}E_\theta$ and displacement $u_b = 0$.

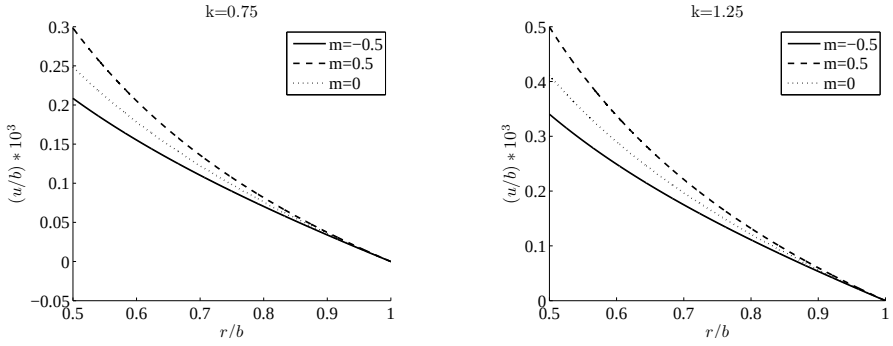

(a) (b)

Figure 15: The variation of the radial displacement for (a) $k = 0.75$ and (b) $k = 1.25$ under prescribed pressure $p = 10^{-3}E_\theta$ and displacement $u_b = 0$.

the disk or cylinder, or a small sphere around the center of a spherical body, within which the assumption of the cylindrical or spherical anisotropy does not apply. This radius is a fraction of the maximum possible outer radius, which is specified by the age of wood, or by technological characteristics of the manufacturing production of the cylinder or sphere.† Otherwise, the anisotropy would be singular at the center (concentration of anisotropy), the elastic modulus in every direction at the center being simultaneously equal to E_r and E_θ, which is physically impossible, and which gives rise to stress singularity at the center [5]. For certain combination of material parameters, the unphysical material overlapping and the displacement singularity could also occur at the center [25-28]. To circumvent this, a small region $r \leq a_o$ around the center is replaced by a transversely isotropic core in the case of a disk or cylinder, or by isotropic core (pith) in the case of a sphere [19,29].

†If a cylinder is produced by deep drawing from a transversely isotropic sheet of metal, there is a minimum possible inner radius of the cylinder specified by the drawing tool and the ductility of the sheet. The outer radius b depends on the thickness of the sheet.

Introducing the parameters

$$\alpha_0 = \begin{cases} 1, \\ 1 - \nu_{rz}^0 \nu_{zr}^0, \\ 1, \end{cases} \qquad \beta_0 = \begin{cases} \nu_0, & \text{for a disk,} \\ \nu_0 + \nu_{rz}^0 \nu_{zr}^0, & \text{for a cylinder,} \\ \nu_0, & \text{for a sphere,} \end{cases} \tag{7.1}$$

and

$$\gamma_0 = \begin{cases} 1, & \text{for a disk,} \\ 1 - \nu_{rz}^0 \nu_{zr}^0, & \text{for a cylinder,} \\ 1 - \nu_0, & \text{for a sphere,} \end{cases} \tag{7.2}$$

it readily follows that, within the core, $\sigma_r = \sigma_\theta = -p_0$, and

$$u(r) = -\frac{\eta_0 p_0}{E_0}\, r\,, \quad (r \le a_0)\,. \tag{7.3}$$

The modulus of elasticity and the Poisson coefficient within a cylindrical core in the plane of isotropy of a disk or cylinder, or within a spherical core in the case of a pressurized solid sphere, are denoted by E_0 and ν_0. The parameter η_0 is defined by

$$\eta_0 = \begin{cases} 1 - \nu_0, & \text{for a disk,} \\ 1 - \nu_0 - 2\nu_{rz}^0 \nu_{zr}^0, & \text{for a cylinder,} \\ 1 - 2\nu_0, & \text{for a sphere.} \end{cases} \tag{7.4}$$

By imposing the continuity of radial displacement at the interface between the core and the outer material, i.e., by equating the displacement expressions from (4.4) and (7.3) at $r = a_0$, it follows that

$$p_0 = \frac{\eta_1 \dfrac{c_0^{-n_1}}{1 - c_0^s} + \eta_2 \dfrac{c_0^{-n_2}}{1 - c_0^{-s}}}{\eta_0 \dfrac{E_\theta^{a_0}}{E_0} + \eta_1 \dfrac{c_0^s}{1 - c_0^s} + \eta_2 \dfrac{c_0^{-s}}{1 - c_0^{-s}}}\, q\,. \tag{7.5}$$

The applied pressure at the boundary $r = b$ is denoted by q, and $c_0 = a_0/b$ is the ratio of the radii of the inner core and the outer boundary. The

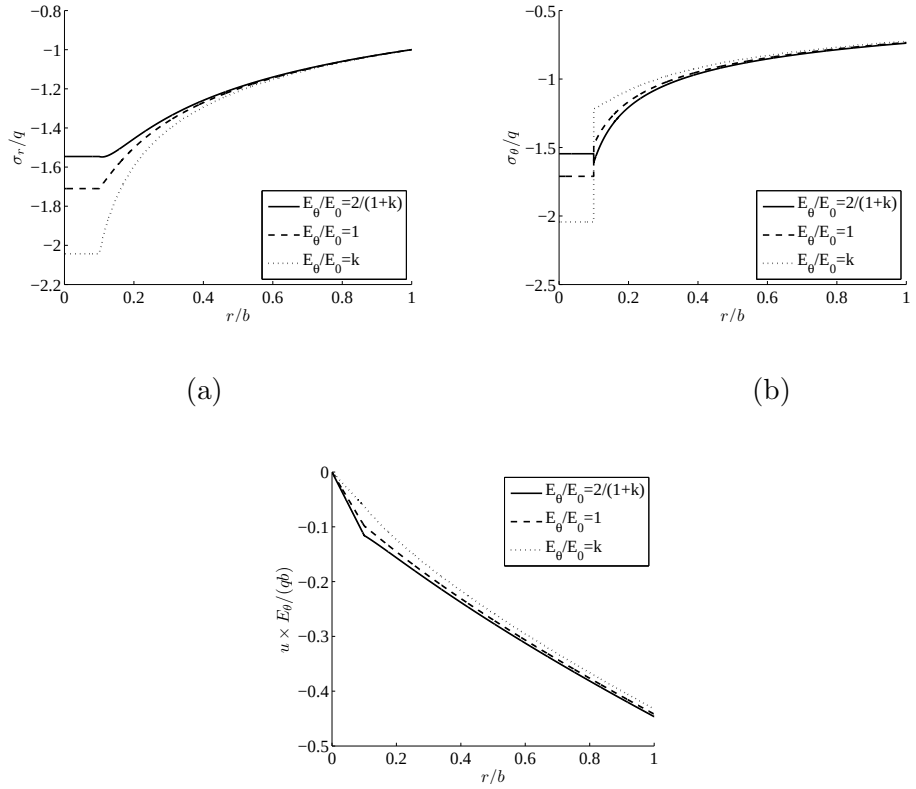

Figure 16: The variation of: (a) radial stress, (b) circumferential stress, and (c) radial displacement in a pressurized thin red oak disk with a pith of radius $a_0 = 0.1b$. The three curves in each case correspond to three different values of the elastic modulus E_0, with $k = 0.532$.

modulus of elasticity $E_\theta(a_0)$ in the material just outside the core is denoted by $E_\theta^{a_0}$.

Although, in general, there is no physical requirement on the continuity of E_0 with either E_r or E_θ across the radius $r = a_0$, three appealing particular cases can be considered by assuming that E_0 is equal to either $E_\theta(a_0)$, $E_r(a_0)$, or their arithmetic mean. This yields

$$\frac{E_\theta^{a_0}}{E_0} = \begin{cases} 1, & \text{if} \quad E_0 = E_\theta^{a_0}, \\ k, & \text{if} \quad E_0 = E_r^{a_0}, \\ \dfrac{2}{1+k}, & \text{if} \quad E_0 = [E_\theta(a_0) + E_r(a_0)]/2. \end{cases} \tag{7.6}$$

Other relationships could hold, dictated by experimental observations for particular materials.

Figure 16 shows the plots of the normalized stresses and the displacement versus the normalized radius of a disk made of red oak (hardwood), for which $E_z = 9.8$ GPa, $E_r = 0.154E_z$, $E_\theta = 0.082E_z$ (thus $k = 0.532$), $\nu_{zr} = 0.35$, $\nu_{rz} = 0.064$, $\nu_{\theta r} = 0.292$, $\nu_{r\theta} = 0.56$, $\nu_{z\theta} = 0.448$, and $\nu_{\theta z} = 0.033$ [30]. If a disk is assumed to be spatially uniform ($m = 0$), this data gives $\alpha = \varphi = 0.532$, $\beta = 0.292$, $n_1 = 0.2706$, $n_2 = 1.7294$, $\eta_1 = 0.4374$, and $\eta_2 = -1.0214$. The radius of the pith is taken to be $a_0 = 0.1b$, and its inplane Poisson ratio is assumed to be the arithmetic mean of the inplane Poisson's ratios of the wood outside of the pith, i.e., $\nu_0 = (\nu_{r\theta}+\nu_{\theta r})/2 = 0.426$. The three curves in each plot correspond to three specified values of E_0, according to (7.6). The strongest discontinuity in the hoop stress across the interface $r = a_0$ occurs in case $E_\theta/E_0 = k$, and the weakest in case $E_\theta/E_0 = 2/(1+k)$ (Fig. 16b). This is so because $k = 0.532$, and the discontinuity in the elastic moduli is $E_0/E_\theta = 1.8797$ in the former, and $E_0/E_\theta = 0.766$ in the latter case. This means that a disk is stiffer in the former case, so that the magnitude of radial stress is greater and the magnitude of radial displacement smaller than in the latter case (dotted curves in Figures 16a and c).

8. CONCLUSION

We have extended in this paper the analysis from [1], applicable to stress boundary conditions, and derived the elastic response of anisotropic and

nonuniform hollow disks, cylinders and spheres under displacement and two types of mixed boundary conditions. Two parameters introduced in [1] play a prominent role in the analysis: the material nonuniformity parameter m, and the parameter φ which accounts for the combined effects of the material anisotropy and nonuniformity. The pressurized solid disk, cylinder, and sphere are then considered, with a small pith around their centers, made of a material with elastic properties different from those of the surrounding material, avoiding possible stress and displacement singularities at the center. The results are applied to hardwood red oak. The discontinuity of the hoop stress across the pith-interface is discussed in terms of the discontinuity of the material properties across the interface. The obtained results may be of interest for the mechanics of wood and functionally graded materials.

Acknowledgments

Research support from the Montenegrin Academy of Sciences and Arts is kindly acknowledged.

References

[1] V.A. Lubarda, On a pressurized cylindrically anisotropic disk or cylinder, and a spherically anisotropic sphere made of a radially nonuniform material. *J. Elasticity* **109** (2012) 103–133.

[2] E. Reissner, Symmetric bending of shallow shells of revolution. *J. math. Mech.* **7** (1958) 121–140.

[3] C.R. Steele, R.F. Hartung, Symmetric loading of orthotropic shells of revolution. *J. Appl. Mech.* **32** (1965) 337–345.

[4] B.W. Shaffer, Orthotropic annular disks in plane stress. *J. Appl. Mech.* **34** (1967) 1027–1029.

[5] S.G. Lekhnitskii, *Theory of Elasticity of an Anisotropic Body.* Mir Publishers (1981).

[6] S.G. Lekhnitskii, *Anisotropic Plates*, 2nd ed. Gordon and Breach, New York (1987).

[7] S.S. Antman, P.V. Negrón-Marrero, The remarkable nature of radially symmetric equilibrium states of aelotropic nonlinearly elastic bodies. *J.*

Elasticity **18** (1987) 131–164.

[8] M. Froli, Distribuzione ottimalle dei moduli elastici in corone circolari non omogenee. *Atti dell'Instituto di Scienza delle Costruzioni dell'Universitá di Pisa* **18** (1987) 13–25.

[9] H.O.K. Kirchner, Elastically anisotropic angularly inhomogeneous media. I. A new formalism. *Phil. Mag. B* **60** (1989) 423–432.

[10] R.M. Christensen, Properties of carbon fibers. *J. Mech. Phys. Solids* **42** (1994) 681–695.

[11] D. Galmudi, J. Dvorkin, Stresses in anisotropic cylinders. *Mech. Res. Comm.* **22** (1995) 109–113.

[12] E. Erdogan, Fracture mechanics offunctionally graded materials. *Compsites Engineering* **5** (1995) 753–770.

[13] H.O.K. Kirchner, Radially inhomogeneous sheets under stress. *J. Appl. Mech.* **62** (1995) 1065–1067.

[14] V.I. Alshits, H.O.K. Kirchner, T.C.T. Ting, Angularly inhomogeneous piezoelectric piezomagnetic anisotropic media. *Phil. Mag. Lett.* **71** (1995) 285–288.

[15] H.O.K. Kirchner, V.I. Alshits, Elastically anisotropic angularly inhomogeneous media II. The Green's function for piezoelectric, piezomagnetic and magnetoelectric media. *Phil. Mag. A* **74** (1996) 861–885.

[16] C.O. Horgan, S.C. Baxter, Effects of curvilinear anisotropy on radially symmetric stresses in anisotropic linearly elastic solids. *J. Elasticity* **42** (1996) 31–48.

[17] T.C.T. Ting, Pressuring, shearing, torsion and extension of a circular tube or bar of cylindrically anisotropic material. *Proc. R. Soc. Lond. A* **452** (1996) 2397–2421.

[18] C.O. Horgan, A.M. Chan, The pressurized hollow cylinder or disk problem for functionally graded isotropic linearly elastic materials. *J. Elasticity* **55** (1999) 43–59.

[19] C.O. Horgan, A.M. Chan, The stress response of functionaly graded isotropic linearly elastic rotating disks. *J. Elasticity* **55** (1999) 219–230.

[20] T.C.T. Ting, The remarkable nature of radially symmetric deformation of spherically uniform linear anisotropic elastic material. *J. Elasticity*

53 (1999) 47–64.

[21] T.C.T. Ting, New solutions to pressuring, shearing, torsion and extension of a cylindrically anisotropic elastic circular tube or bar. *Proc. R. Soc. Lond. A* **455** (1999) 3527–3542.

[22] T.C.T. Ting, The remarkable nature of cylindrically orthotropic elastic materials under plane strain deformations. *Q. Jl. Mech. appl. Math.* **52** (1999) 387–404.

[23] Z.-H. Jin, R.C. Batra, Some basic fracture mechanics concepts in functionally graded materials. *J. Mech. Phys. Solids* **44** (1996) 1221–1235.

[24] R.C. Batra, G.L. Iaccarino, Exact solutions for radial deformations of a functionally graded isotropic and incompressible second-order elastic cylinder. *Int. J. Nonlin. Mechanics* **43** (2008) 383–398.

[25] Fosdick, R.L., Royer-Carfagni, G.: The constraint of local injectivity in linear elasticity theory. Proc. R. Soc. Lond. A **457**, 2167-2187 (2001).

[26] Aguiar, A.R.: Local and global injective solution of the rotationally symmetric sphere problem. J. Elasticity **84**, 99-129 (2006).

[27] Aguiar, A.R., Fosdick, R.L., Sánchez, J.A.G.: A study of penalty formulations used in the numerical approximation of a radially symmetric elasticity problem. J. Mech. Matar. Struct. **3**, 1403–1427 (2008).

[28] Fosdick, R.L., Freddi, F., Royer-Carfagni, G.: Bifurcation instability in linear elasticity with the constraint of local injectivity. J. Elasticity **90**, 99-126 (2008).

[29] Tarn, J.-Q.: Stress singularity in an elastic cylinder of cylindrically anisotropic materials. J. Elasticity **69**, 1–13 (2002).

[30] D.W. Green, J.E. Winandy, D.E. Kretschmann, Mechanical properties of wood. In: *Wood Handbook – Wood as an Engineering Material* (Centennial edition), pp. 4-1–45. Forest Products Laboratory, United States Department of Agriculture Forest Service, Madison, Wisconsin (2010).